RESEARCH ARTICLE | MAY 03 2024

Spatial evolution of the double-wave-group focusing influenced by the co- and counter-propagating current ⊘

Kanglixi Ding (丁康礼玺) ⓘ ; Binzhen Zhou (周斌珍) ⓘ ; Yi Xiao (肖义) ⓘ ; Lei Wang (王磊) ✉ ⓘ ; Huabin Shi (施华斌) ⓘ

Check for updates

View Online   Export Citation

Articles You May Be Interested In

Influence of uniform currents on nonlinear characteristics of double-wave-group focusing

Physics of Fluids (March 2024)

Nonlinear statistical characteristics of the multi-directional waves with equivalent energy

Physics of Fluids (August 2023)

Instability mechanism of shear-layered fluid in the presence of a floating elastic plate
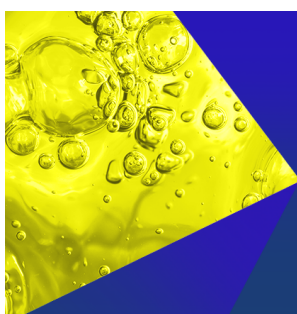
Physics of Fluids (February 2023)

28 November 2025 04:30:49

Spatial evolution of the double-wave-group focusing influenced by the co- and counter-propagating current

View Online   Export Citation   CrossMark

Kanglixi Ding (丁康礼玺),[1] [iD] Binzhen Zhou (周斌珍),[1] [iD] Yi Xiao (肖义),[1] [iD] Lei Wang (王磊),[1,2,3,a] [iD]
and Huabin Shi (施华斌)[4] [iD]

AFFILIATIONS

[1]School of Civil Engineering and Transportation, South China University of Technology, Guangzhou 510641, China
[2]Department of Civil and Environment Engineering, The Hong Kong Polytechnic University, Hong Kong 999077, China
[3]Guangxi Key Laboratory of Beibu Gulf Marine Resources, Environment and Sustainable Development, Beihai 536000, China
[4]State Key Laboratory of Internet of Things for Smart City and Department of Ocean Science and Technology, University of Macau, Taipa, Macao, China

[a]Author to whom correspondence should be addressed: wangleimme@scut.edu.cn

ABSTRACT

Wave–current interaction has always been a challenging topic in fluid mechanics. The research on bimodal waves has received much more attention recently, but their evolutions influenced by underlying currents are not yet clear. This study aims to investigate the effects of co- and counter-propagating currents on spatial evolution using a fully nonlinear wave-current tank based on the high-order spectral method. The process of the wave focus is significantly shortened by the counter-propagating current, resulting in a sharper crest focus, followed by the trough focus. Concurrently, the decrease in the total envelope height and width is accelerated before wave focus and then the increase is decelerated, accompanied by a delay in the envelope profile transition from the backward-leaning to the forward-leaning. The co-propagating current exhibits the opposite phenomenon. The analysis of the spectral energy distribution aids in clarifying the variation of the envelope profile. The energy redistribution, characterized by a downshift of the frequency band, and a decreased energy distribution at the second peak, along with the slightly larger value of the root mean square frequency, indicates that the energy back-flow is obstructed by the counter-propagating current. These findings contribute to our understanding of the current effect on the focused double-wave-group, providing valuable insights for future research and applications in this field.

I. INTRODUCTION

With more and more frequent marine activities, marine environmental safety has become one of the most important issues in the field of ship and ocean engineering.[1,2] Wave–current interaction is one of the main external factors, posing a serious threat to marine engineering equipment, which receives increasing attention from experts and scholars.[3,4] In addition to the unimodal waves,[5,6] the bimodal sea state, usually occurring in the intersection of the estuary and the open sea or the passage of typhoons, is also more likely to deduce extreme waves as well.[7,8] However, the evolutionary characteristics are not identical to that in the unimodal sea state.[9,10] Therefore, studying the influence of the currents on the spatial evolution of extreme waves in the bimodal sea states is of great significance for the understanding of the physical mechanism of extreme waves.

Generous efforts have been made in the variation of the extreme wave profile. Compared to the linear prediction of the two adjacent troughs symmetrical relative to the maximum crest,[11] nonlinear interaction results in an abnormal rise in the amplitude and asymmetry of the extreme wave.[12] This was observed in single wave packets,[13] random wave fields,[14] and other water wave conditions.[15,16] Gibbs and Taylor[17] proposed a local envelope width to measure the horizontal contraction of the extreme waves. They also found that the extreme wave was shaped as a "wall of water" due to the nonlinear contraction, which was proven by the analytical results of Adcock et al.[18] Afterward, other parameters were put forward to describe the strongly nonlinear waves, even considering wave breaking.[19,20] Adcock et al.[21,22] proposed two parameters to assess the horizontal asymmetry influenced by the nonlinear dynamic, which was widely applied.

One is β, defined as a ratio of the envelope height at half of the average characteristic period relative to the maximum height, and the other is σ, defined as the envelope width at 80% of the maximum peak height of the wave envelope. They also pointed out that the largest wave with sufficiently large steepness inclines to move to the front of the wave group.[22] Tang et al.[23] proved that nonlinear interaction indeed leads to the increase in horizontal asymmetry as well as nonlinear contraction with wave steepness increasing in the open ocean. Furthermore, the spatial evolution of extreme waves was investigated by Tang et al.[24,25] They found that horizontal asymmetry reaches the maximum value with the occurrence of the largest peak and then declines to a near-zero steady-state value.

Recently, the influence of currents on the nonlinear characteristics of wave groups has attracted more attention. The wavelength was proven to be stretched by the co-propagating current but compressed by the counter-propagating current.[26,27] As a result, extreme waves were observed triggered more frequently in the counter-propagating current.[28] In circumstances such as random wave field,[29] Peregrine breather[30] as well as the focused wave[31,32] colliding with the counter-propagating current, wave profiles were more intensively altered relative to the non-current condition. It manifested in the amplification of wave amplitude, the enhancement of envelope asymmetry, and the increase in wave steepness. Merkoune et al.[32] pointed out that the changes in wave profile were accompanied by more energy transfers to the relatively high-frequency partition, resulting in a broadened frequency bandwidth. Concerning the focused waves, Wang et al.[33] found that the focused position and time were lagged by the co-propagating current, but otherwise for the counter-propagating current. Moreover, the altered focused position and time seemed to be correlative with the wave group velocity accelerated or decelerated by the currents.[34,35]

The aforementioned study mainly focused on the unimodal waves. However, 33% of the open sea was observed to exhibit a bimodal behavior.[36,37] Intermodal distance (ID) and sea-swell energy ratio (SSER) were defined to describe the energy distribution of the bimodal sea state. Their changes had a significant impact on the nonlinear characteristic of double-wave-group focusing, different from that of single-wave-group focusing.[38] A closer ID (ID < 0.1) or asymmetrical spectrum distribution (SSER $\neq$ 1.0) was pointed to activate more nonlinearities,[39,40] manifesting as the increase in either extra amplitude or the occurrence of extreme waves. Through the analysis of the measured data, Halsne et al.[7] reported a 45% rise in significant wave height when the bimodal sea state collided with a counter-propagating current. Based on this, Zhou et al.[8] investigated the effect of the uniform current on the double-wave-group focusing. Three ranges were found in the focused amplitude influenced by current, consisting of the reduction in co-propagating current, the rise in weakly counter-propagating current, and the re-decrease in strongly counter-propagating current. For the strongly counter-propagating current, distinctive nonlinear characteristics were triggered.

Great progress is dedicated to the nonlinear characteristics at a prescribed position.[8,41] However, the influence of the current on the double-wave-group focusing is appreciably distinctive at different positions, impossible to predict the evolutionary features only by those in one position. Therefore, the spatial evolution of the double-wave-group focusing influenced by the co- and counter-propagating current is numerically simulated. The novelties are threefold. First, in addition to the focused parameters (e.g., actual focused position, focused time,

and maximum magnitude), the occurrence of the crest focus and trough focus influenced by various currents is also clarified. Second, the concentration of wave energy around the largest crest as well as the horizontal asymmetry of the envelope due to the wave-current interaction is revealed. Third, the spatial evolution of the energy redistribution and two typical characteristic frequencies is investigated to explain changes in the wave envelope under the influence of various currents.

The rest of this paper is arranged as follows: The numerical setup of the wave-current model is introduced in Sec. II, along with the description of the wave-current configuration. The evolution of the envelope profile and the spectral energy distribution influenced by co- and counter-propagating various currents are analyzed in Secs. III and IV, respectively. The main conclusions are summarized in Sec. V.

II. NUMERICAL MODEL SETUP
A. Wave–current coupling model

The high-order spectral (HOS) method,[42] with significant advantages in efficiency as well as accuracy using the Fast Fourier Transform (FFT) to solve the velocity potential and derivative terms, is employed in this study, in which the incompressible, inviscid, and irrotational fluid within the two-dimensional field D satisfies the Laplace equation

$$\frac{\partial^2 \Phi}{\partial x^2} + \frac{\partial^2 \Phi}{\partial z^2} = 0 \quad \text{in } D, \tag{1}$$

where Φ is the velocity potential within the domain. The origin of the coordinate system is located at the intersection of the wavemaker boundary and the still water line (SWL), in which the x-axis lies on the SWL, along with the direction of the wave propagation defined as positive, and the z-axis is vertical to the SWL and its positive direction is assumed upward.

When introducing a steady, irrotational, and uniform current with a horizontal velocity of U, the water velocity potential in the fluid domain can be composed of three parts:[43] the free surface spectral potential Φ_f^s, the addition velocity potential Φ_{add},[42] and the velocity potential driven by the uniform current

$$\Phi(x, z, t) = \Phi_f^s(x, t) + \Phi_{add}(x, z, t) + Ux. \tag{2}$$

Consequently, the corresponding free surface kinematic and dynamic boundary conditions can be revised by introducing the effect of the current[31]

$$\frac{\partial \eta}{\partial t} = \left(1 + \left|\frac{\partial \eta}{\partial x}\right|^2\right)\frac{\partial \Phi_f^s}{\partial z} + \frac{\partial \Phi_{add}}{\partial z} - \left(\frac{\partial \Phi_f^s}{\partial x} + \frac{\partial \Phi_{add}}{\partial x} + U\right)\frac{\partial \eta}{\partial x}$$
$$z = \eta(x, t), \tag{3}$$

$$\frac{\partial \Phi_f^s}{\partial t} = -g\eta + \frac{1}{2}\left(1 + \left|\frac{\partial \eta}{\partial x}\right|^2\right)\left(\frac{\partial \Phi_f^s}{\partial z}\right)^2 - \frac{1}{2}\left|\frac{\partial \Phi_f^s}{\partial x}\right|^2 - \frac{1}{2}|\nabla \Phi_{add}|^2 - \frac{1}{2}|U|^2$$
$$- \frac{\partial \Phi_f^s}{\partial x} \cdot \frac{\partial \Phi_{add}}{\partial x} - U\frac{\partial(\Phi_f^s + \Phi_{add})}{\partial x} - \frac{\partial \Phi_{add}}{\partial t} \quad z = \eta(x, t), \tag{4}$$

where η denotes the water surface elevation.

The bottom boundary condition, wavemaker condition, and initial condition are given as

$$\frac{\partial \Phi}{\partial z} = \frac{\partial \Phi_f^s}{\partial z} + \frac{\partial \Phi_{add}}{\partial z} = 0 \quad z = -h, \tag{5}$$

$$\frac{\partial S}{\partial t} + U = \frac{\partial \Phi_{add}}{\partial x} + U \quad x = 0, \tag{6}$$

$$\begin{cases} \eta(x, t=0) = 0, \\ \Phi_f^s(x, t=0) = 0, \\ \Phi_{add}(x, z, t=0) = 0, \end{cases} \tag{7}$$

where h denotes the water depth, and S is the displacement of the wavemaker.

The prescribed additional velocity potential Φ_{add} can be obtained from the wavemaker theory[44] based on our expected waves. The free surface velocity potential Φ_f^s and the water surface elevation η are to be solved using the traditional high-order spectral method proposed by Dommermuth and Yue[45] and West et al.[46] The absorbing zone is described by a local modification of pressure at the free surface,[42,47] in which the damping coefficient is defined as a third-order polynomial.

A numerical wave–current tank is established, as illustrated in Fig. 1. The computational domain is 32 m long (L_x) and 1 m deep (h). A wavemaker is set at the left side to generate waves and an absorbing zone is at the end to reduce the reflected waves. When the underlying current goes in the same direction as the wave group, it is defined as co-propagating, otherwise, it is counter-propagating.

To ensure the spatial, temporal, and nonlinear order resolution is sufficient to accurately capture the complicated nonlinear physical evolution, refer to the convergence analysis performed in Ref. 8. Per wavelength is discretized with 50 modes in the x-direction, with time step adopted as 0.02 s and the nonlinear order expanded up to 5. The experiment conducted by Liu et al.[48] is used to validate the established numerical model. The water surface elevation at $x = 15$ m between the numerical results and the experimental data is compared in Fig. 2, considering the non-current state, co-propagating current state, and counter-propagating current state. The good agreement indicates the ability of the numerical model to accurately simulate wave–current interactions.

B. Wave–current configuration

The bimodal sea state is characterized by sea-swell energy ratio (SSER) and intermodal distance (ID), which are defined by[49]

$$\begin{cases} \mathrm{SSER} = \dfrac{m_{02}^2}{m_{01}^2}, \\ \mathrm{ID} = \dfrac{f_{P2} - f_{P1}}{f_{P1} + f_{P2}}, \end{cases} \tag{8}$$

where m_0 is the 0-order spectral moment and f_p is the peak frequency. The subscripts 1 and 2 denote the wave parameters of the swell system (corresponding to the wave group with a relatively low peak frequency) and wind–sea system (corresponding to the wave group with a relatively higher peak frequency), respectively. Case A and case B represent the cases corresponding to a focused single wave group with a relatively low peak frequency and one with a relatively higher peak frequency.

The double-wave-group focusing (named case AB in our study) is generated based on their wavemaker signals, which are the linear superposition of the corrected ones of the two corresponding single-wave-group focusing.[8,40] For each single-wave-group focusing (case A and case B), the iterative method[50] is applied to correct the deviation of the actual focused position (i.e., x_{ab}) relative to the assumed (i.e., x_b), as well as the focused time.

In the present study, SSER = 1.00 and ID = 0.10 (listed in Table I) are set, where A_b is the assumed focused amplitude, and k_p is the peak wavenumber associated with the peak frequency through the dispersion relation. The assumed focused position x_b is taken as 15 m, along with the assumed focused time t_b taken as 50 s. The advanced JONSWAP spectrum proposed by Goda[51] is employed in this study. The frequency bandwidth is taken from 0.5 to 2.0 Hz uniformly distributed among 192 wave components. The peak elevation factor γ is valued at 3.3.

The current velocity normalized by c_{gz_0} (valued at 0.64 m/s in this study), the group velocity in the bimodal sea state without current,[49] is chosen (listed in Table II) to interact with the wave group. The actual focused position x_{ab} and the actual focused time t_{ab} influenced by the current are also given.

C. Analytical parameters

1. Dimensionless temporal and spatial parameters

(1) $(t - t_{ab\_0})/T_{z\_0}$, a normalized propagation time, is used to describe the number of the characteristic period relative to the actual focused time, in which T_z represents the average zero-crossing period,[49] and the subscript "_0" denotes the corresponding variables in the non-current state.

(2) X, a normalized propagation distance, is used to denote the number of the characteristic wavelength relative to the actual focused position. It is defined as
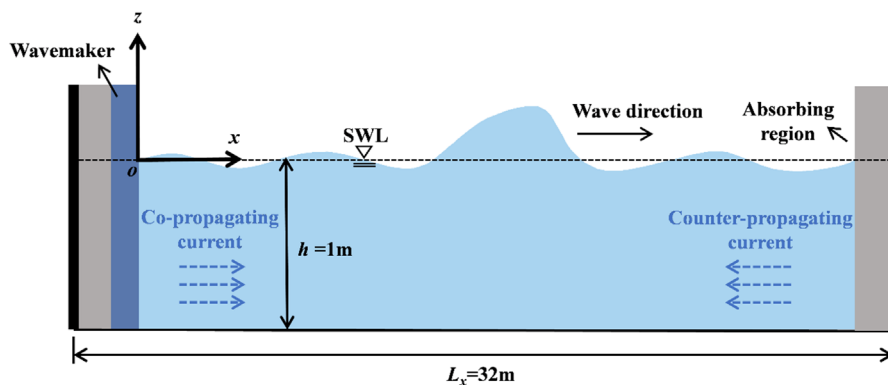

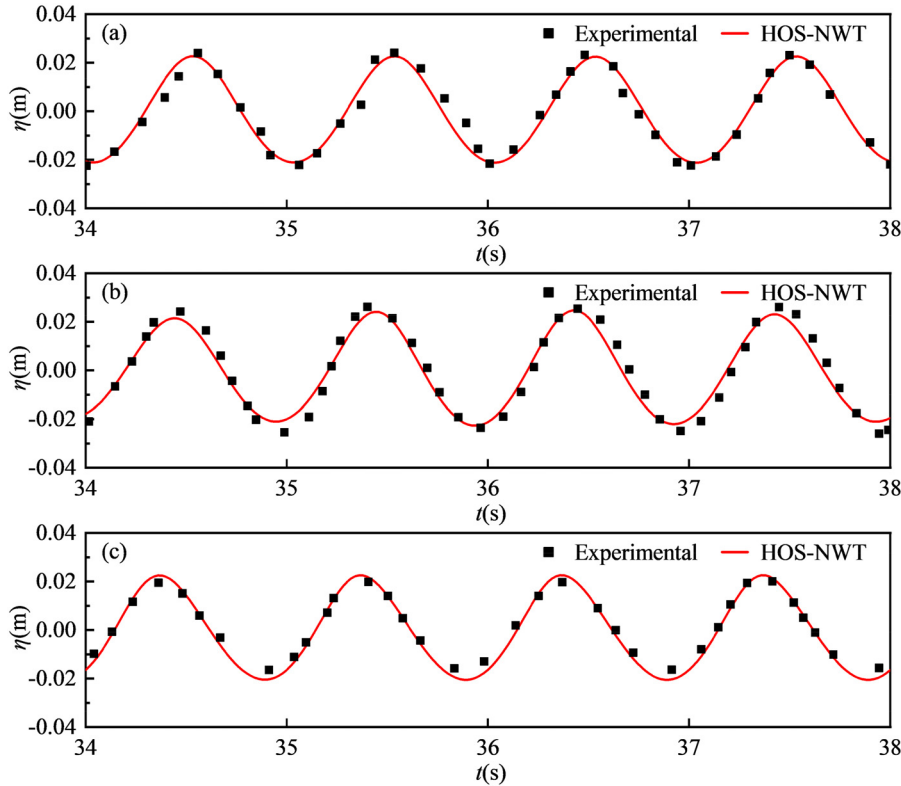FIG. 1. Sketch of the numerical wave–current tank.

FIG. 2. Comparison of the water surface elevation between numerical results and experimental data with various current configurations. (a) $U = 0.00$ m/s, (b) $U = -0.139$ m/s, and (c) $U = 0.135$ m/s.

TABLE I. Detailed parameters of the wave configuration.

Case A			Case B			Case AB		
A_{b1} (m)	f_{p1} (Hz)	$k_{p1}A_{b1}$	A_{b2} (m)	f_{p2} (Hz)	$k_{p2}A_{b2}$	A_b (m)	ID	SSER
0.025	0.903	0.082	0.025	1.103	0.122	0.050	0.10	1.00

TABLE II. Configuration of uniform currents and the actual focused information.

U/c_{gz_0}	0.15	0.10	0.05	0.00	−0.05	−0.10	−0.15
x_{ab} (m)	21.38	19.62	16.74	14.16	12.64	10.36	8.36
t_{ab} (s)	53.64	53.02	50.68	48.40	47.78	45.56	43.46

$$X = (x - x_{ab})/\lambda_z, \tag{9}$$

where λ_z corresponds to the wavelength in different undergoing currents, obtained through the dispersion relation considering the effect of the current.[27]

2. Wave envelope

Wave envelope $E(t)$ is beneficial to reflect the evolution of the non-stationary process such as extreme waves over a bathymetry[52,53] as well as the wave group focusing.[54] Figure 3 shows the spatial evolution

of the upper and lower wave envelopes obtained by the peak detection method. The non-current configuration is taken as an example. The vertical axis η/A_b represents the normalized water surface elevation, and E/A_b represents the normalized value of the wave envelope.

To evaluate the effect of various currents on the evolution of wave envelope, two parameters are introduced.

(1) a_{up} and a_{low}, the height ratio of the extreme values of the upper and lower envelopes relative to that in the absence of the underlying current, are defined as

$$a_{up} = |E_{up}|/|E_{up\_0}|, \quad a_{low} = |E_{low}|/|E_{low\_0}|, \tag{10}$$

where the subscripts "up" and "low" represent the extreme values of the upper and lower envelopes (i.e., corresponding to the maximum and the minimum values), respectively. Once the value of this ratio is larger than 1.0, it represents the extreme value strengthened by the undergoing current compared to the conditions without currents, otherwise, it is suppressed.

(2) Δt_{up} and Δt_{low}, the occurrence time deviation of the extreme values of the upper and lower envelope from that in the non-current state, are defined as

$$\Delta t_{up} = t_{up} - t_{up\_0} \quad \Delta t_{low} = t_{low} - t_{low\_0}. \tag{11}$$

The positive value of Δt denotes that the appearance of the extreme value lags behind that of the corresponding non-current state, while the negative denotes the early appearance.
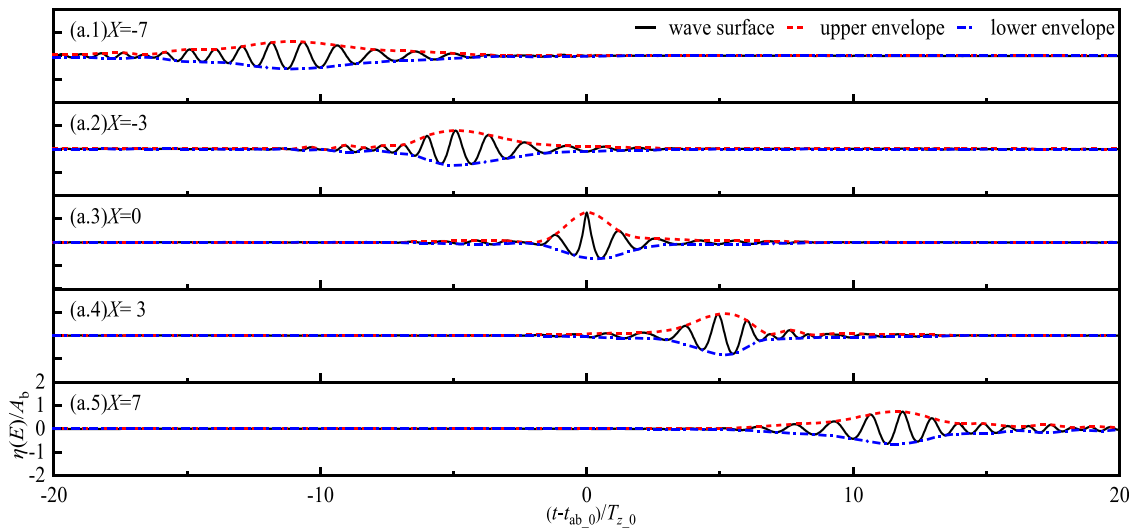
FIG. 3. Spatial evolution of the upper and lower envelopes in a non-current state.

3. Asymmetric parameter

The wave profile can reflect its nonlinearity, and it is true for the wave envelope. Two parameters to be used in the coming analysis are defined hereafter, as illustrated in Fig. 4.

(1) β, a ratio of the envelope height at $T_{z\_0}/2$ relative to the maximum height [as illustrated in Fig. 4(a)], can be written as[21]

$$\beta_p = \frac{|E_p|}{|E_{max}|}, \quad \beta_f = \frac{|E_f|}{|E_{max}|}, \quad (12)$$

where the subscripts p and f denote the preceding and following wave envelopes, respectively. Note that, the preceding and following are defined relative to the direction of the wave propagation hereafter.

β_{sum}, the sum of the relative height of the preceding and following envelopes, can be used to express the energy concentration of the wave group around the largest wave crest, written as

$$\beta_{sum} = \beta_p + \beta_f. \quad (13)$$

The larger the value of β_{sum}, the more concentrated the energy of the wave group is.

(2) σ is defined as the envelope width at 80% of the maximum peak height of the wave envelope [illustrated in Fig. 4(b)]. Here, σ_{sum} and $\Delta\sigma$ are also introduced to measure their sum and difference of the preceding and following wave envelopes, written as[24]

$$\sigma_{sum} = \sigma_p + \sigma_f, \quad (14)$$
$$\Delta\sigma = \sigma_p - \sigma_f. \quad (15)$$

Here, σ_{sum} reflects the horizontal width of the envelope at different positions in the evolutionary process. $\Delta\sigma$ can be used to compare the asymmetry of the preceding and following envelopes. The positive value indicates a backward-leaning profile, and the negative value indicates a forward-leaning profile.

4. Characteristic frequency

(1) f_{rms}, the root mean square frequency (defined as the radius of gyration as the spectra rotate around the y-axis[55]) can be used to measure the energy distribution in the frequency domain during the wave propagation, given as

$$f_{rms} = \sqrt{\frac{m_2}{m_0}}, \quad (16)$$

where m_2 denotes the second-order spectral moment. The larger value of f_{rms} indicates more higher-frequency components appearing.

(2) f_v, defined as the corresponding frequency corresponding to the valley between the two peaks in the frequency spectrum, is illustrated in Fig. 5 in blue, along with the corresponding energy distribution a_v.

(3) f_{nd}, defined as the second peak frequency, is illustrated in Fig. 5 in red with the corresponding energy distribution a_{nd}. Note that this parameter is different from the input peak frequency of the wind–sea system f_{P2} since this parameter will be variable in the evolution of the wave propagation for nonlinear interactions between fluids.

III. EVOLUTION OF WAVE PROFILE INFLUENCED BY CURRENTS

A. Upper and lower envelopes

Figure 6 compares the spatial evolution of the upper [Fig. 6(a)] and lower envelopes [Fig. 6(b)] in the presence of various currents, where the vertical axis is normalized by the assumed focused amplitude of the double-wave-group focusing. The peak of the envelope enhances first and then declines with the wave group propagating from focus to defocus. Additionally, the presence of the underlying current drives the wave group off the occurrence time in the absence of the current, irrespective of the upper or the lower envelope.
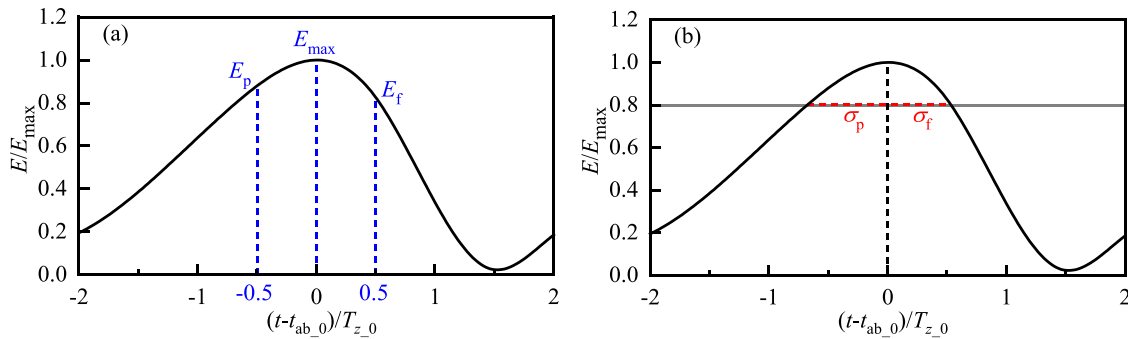
FIG. 4. Illustration of the asymmetric parameters of wave envelope. (a) β and (b) σ.

In Fig. 6(a.1), at the initial stage, even if the co-propagating modifies the upper envelope being narrower and steeper, it lags the upper envelope in the non-current or counter-propagating current. After the swell (the wave group with a relatively low peak frequency) begins to converge with the wind sea (the wave group with a relatively higher peak frequency) [Fig. 6(a.2)], the counter-propagating current drives the contraction of the envelope profile in the horizontal direction. Till the focused position [Fig. 6(a.3)], the sufficient concentration of energy attributes to maximum peak values and the narrowest envelope profiles. Passing by the wave focus [Figs. 6(a.4) and 6(a.5)], the evolution of the components with different propagation velocities being spread out is impaired by the counter-propagating current, causing the envelope profile more slowly returning to the original state. In the evolutionary process of focus and defocus, the spatial evolution of the envelope profile is not an exact mirror regarding the focused position, manifested as the asymmetry property of the envelope profile shifting from forward to backward due to the various wave–current interactions. In the lower envelope [Fig. 6(b)], the position where the maximum magnitude appears is drift, manifested as the phenomenon of the advanced influenced by the co-propagating currents and delayed by the counter-propagating currents. In the co-propagating current, the trough focus occurs earlier than the crest focus, while in the counter-propagating current, the trough focus occurs later than the crest focus.
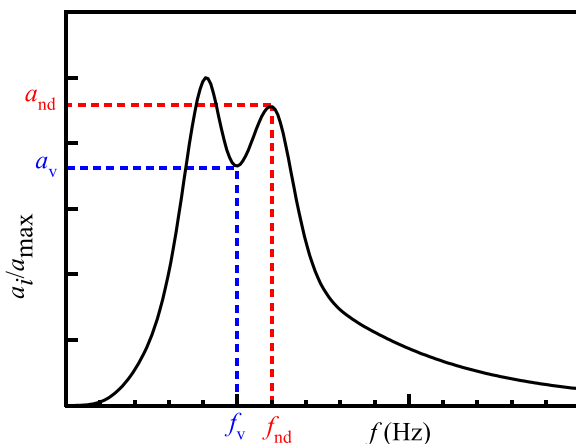

FIG. 5. Characteristic frequencies and their corresponding energy distributions.

B. Magnitudes and their occurrence time

The spatial evolution of the maximum magnitude and the corresponding occurrence time of the upper and lower envelopes influenced by various currents are given in Fig. 7.

For the upper envelope [Fig. 7(a.1)], at the initial stage, the maximum magnitude a_{up} in the co-propagating current is larger than that in the counter-propagating current. Meanwhile, the larger the value of the co-propagating current velocity, the larger the value of the maximum magnitude, and the opposite for the counter-propagating current. At the three times characteristic wavelength before the wave focus, a_{up} reaches a maximum value of 1.25 in the co-propagating current with the velocity $U/c_{gz\_0} = 0.15$ and a minimum value of 0.84 in the counter-propagating current with the velocity $U/c_{gz\_0} = -0.15$. Till the focused position, a_{up} in the co-propagating current decreases to the value of less than 1.0, but most of that in the counter-propagating current increases to the value larger than 1.0, except for the state with $U/c_{gz\_0} = -0.15$, associated with the blocking effect reported in our work.[8] As these two wave groups are gradually separated, the value of a_{up} tends to be stable around 1.0, finally with values in the counter-propagating currents larger than those in the co-propagating currents. Although the wave group velocity in the counter-propagating current is slowed down, the nonlinear interaction is excited in the process of focus and defocus, manifested in the rapid variation of the energy transfer in the maximum magnitude near the focused position. For the lower envelope [Fig. 7(b.1)], all of the occurrence positions up-crossing or down-crossing the relative equivalent value (i.e., $a_{low} = 1.0$) lag behind those in the upper envelope. It is related to the occurrence order of the crest focus and the trough focus under the effect of the water current.

Concerning the deviations of extreme value occurrence time relative to that in the non-current state [Figs. 7(a.2) and 7(b.2)], the co-propagating current inclines to be larger than 0, but the counter-propagating current prefers negative. The co-propagating current delays the occurrence of the extreme values of the upper and lower envelopes, while the impact of the counter-propagating current is the opposite. Additionally, Δt_{up} and Δt_{low} tend to slightly decrease as the wave propagation in the co-propagating current, but they almost maintain constant values in the counter-propagating current. The greater the value of the current velocity, the greater the deviation of the occurrence time of the extreme values. This can be explained by the fact that the counter-propagating current excites the nonlinearity within the fluids, but the co-propagating current does the opposite.
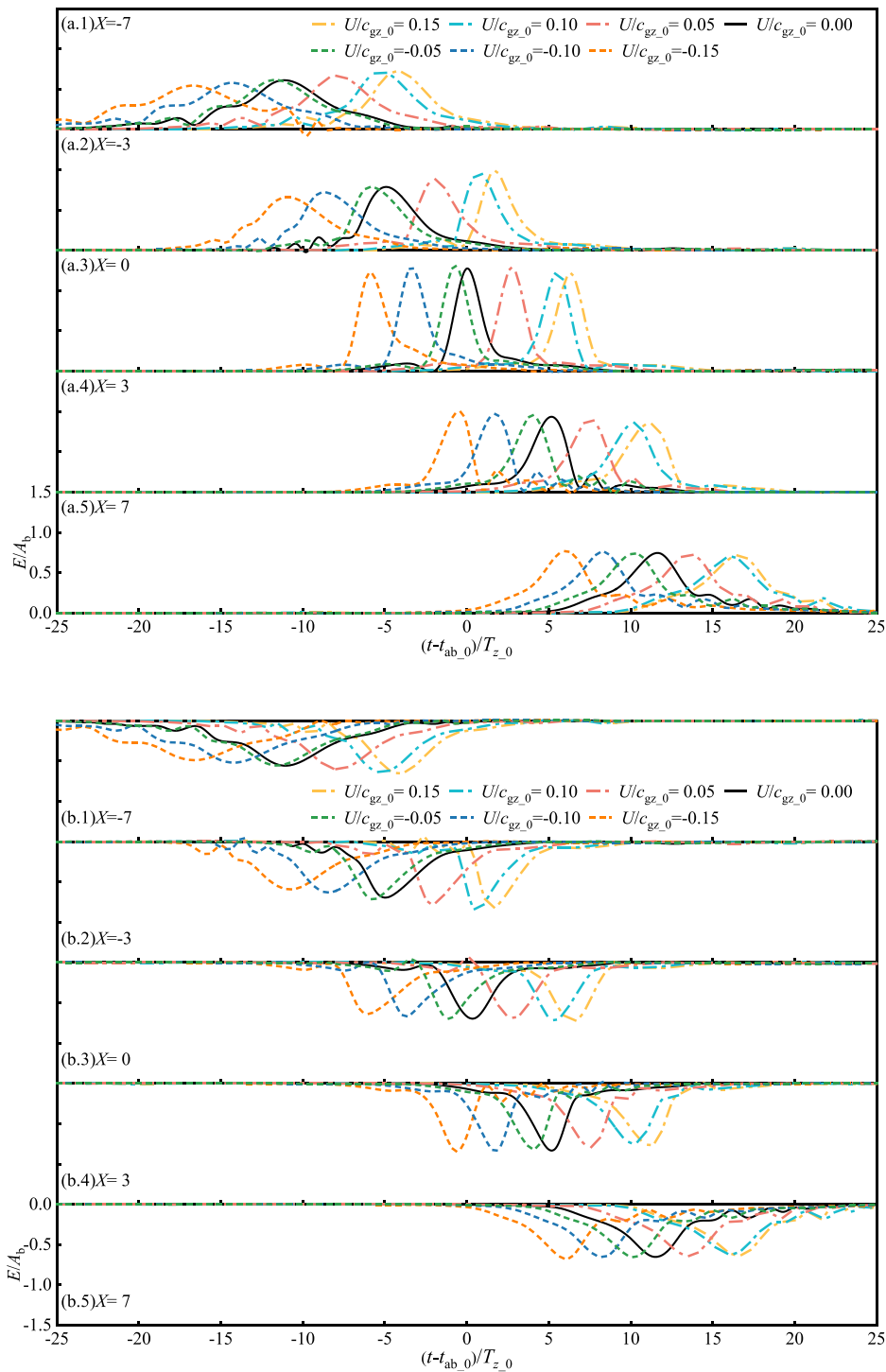
FIG. 6. Evolution of wave envelopes influenced by water currents with various velocities. (a) Upper envelope and (b) lower envelope.

C. Asymmetry

Figure 8 presents the sum of the preceding and following envelope heights [obtained from Eq. (13)], including the upper and lower envelopes, to investigate the concentration of wave energy around the largest crest. For the upper envelope [Fig. 8(a)], the initial values of $\beta_{\text{sum\_up}}$ are more than 1.9, irrespective of the co- or counter-propagating current. As the wave propagates, $\beta_{\text{sum\_up}}$ dramatically declines with the co-propagating current enhancement, but a slight
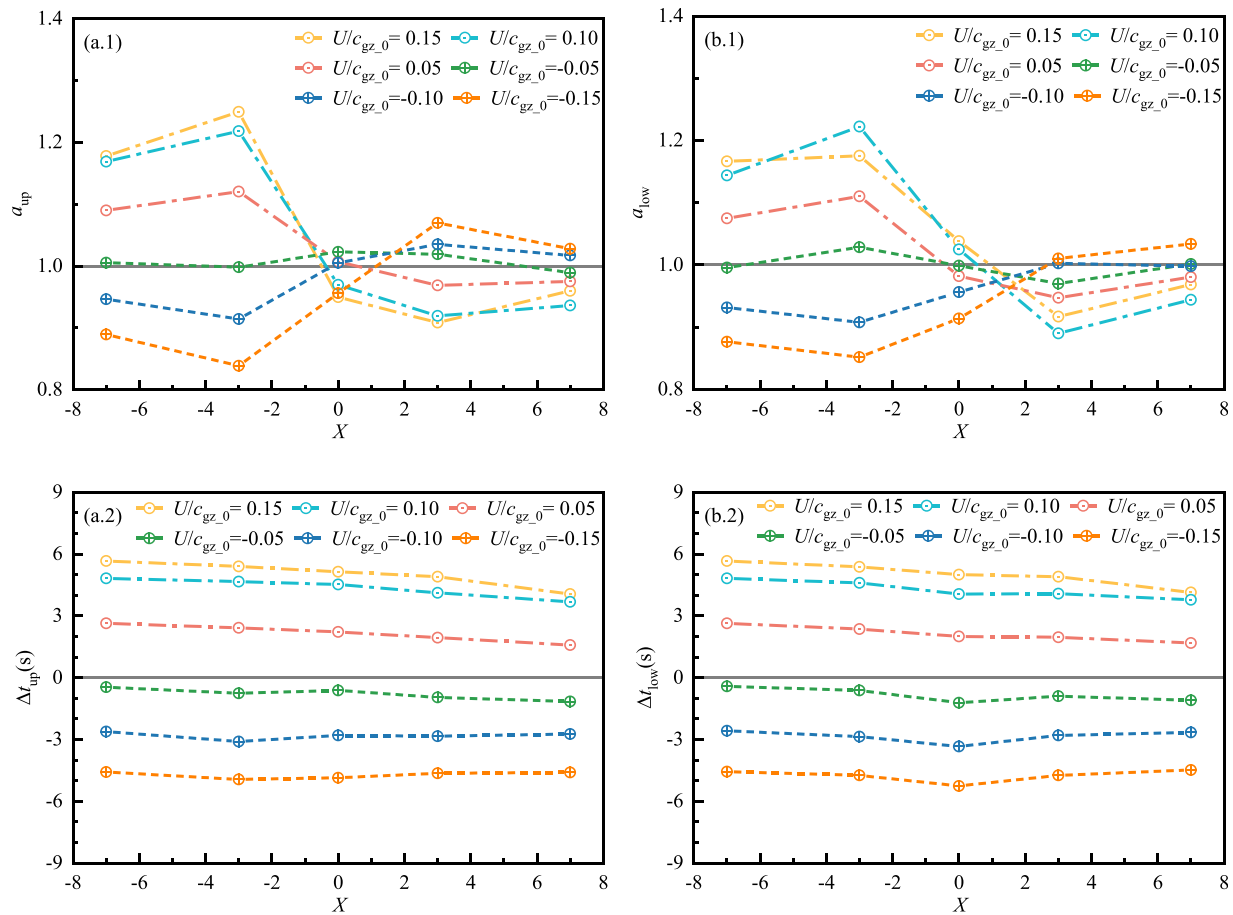
FIG. 7. Influence of the current on the maximum magnitudes (1) and their corresponding occurrence time (2) relative to those in a non-current state. (a) Upper envelope and (b) lower envelope.

reduction in the counter-propagating current, reflecting that the energy of the adjacent components tends to converge toward the largest crest influenced by the co-propagating current. When approaching the focused position, all β_{sum_up} decreases to their minimum values. Meanwhile, a stronger counter-propagating current induces a larger magnitude of the decrease within such a limited distance. After that, β_{sum_up} turns out to increase up to above 1.8 till the wave groups are peeled off from each other. This process is accelerated by the co-propagating current but obstructed by the counter-propagating current. Concerning the variation of the lower envelope [Fig. 8(b)], the wave–current interaction is manifested as a relatively smaller minimum in the co-propagating current before the wave focus but opposite in the counter-propagating current. Since the measured points are selected in the process of the wave components focused on the crest, the ambiguous variation trend of β_{sum_low} in various currents is reasonable.

Figure 9 summarizes the spatial evolution of the envelope width σ_{sum} in the horizontal direction [obtained by Eq. (14)]. In Fig. 9(a), as the value of the current velocity turns from positive (the co-propagating current) to negative (the counter-propagating current), σ_{sum_up} keeps getting larger, that is, the envelope width is getting broadened.

Then, σ_{sum_up} continues to reduce around 0.9 till the focused position. It is consistent with the observation based on the detection of the natural ocean that the minimum of the envelope width occurred at the focused position.[21,24] Meanwhile, the decrease rate of σ_{sum_up} is speeded up with the increase in the counter-propagating current velocity. Behind the focused position, the envelope width becomes broadened as the two wave groups are separated. In this process, the extending of the envelope in the co-propagating current is faster than that in the counter-propagating current, but the increase rate is much lower than the descent rate before the wave focus. In addition, the departure of the envelope width at the position seven times the characteristic wavelength in front of the focused position (i.e., $X = -7$) and that behind the focused position (i.e., $X = 7$) is enlarged by the counter-propagating current, which may be attributed to nonlinearities activated by the counter-propagating wave–current interaction can still modify the envelope profile. A distinct difference in the lower envelope [Fig. 9(b)] is that the narrowest envelope width (i.e., the minimum of σ_{sum_low}) occurs before the focused position in the co-propagating current but opposite in the counter-propagating current.

The total envelope width of the preceding and the following can describe the energy gathering around the maximum crest, but it is
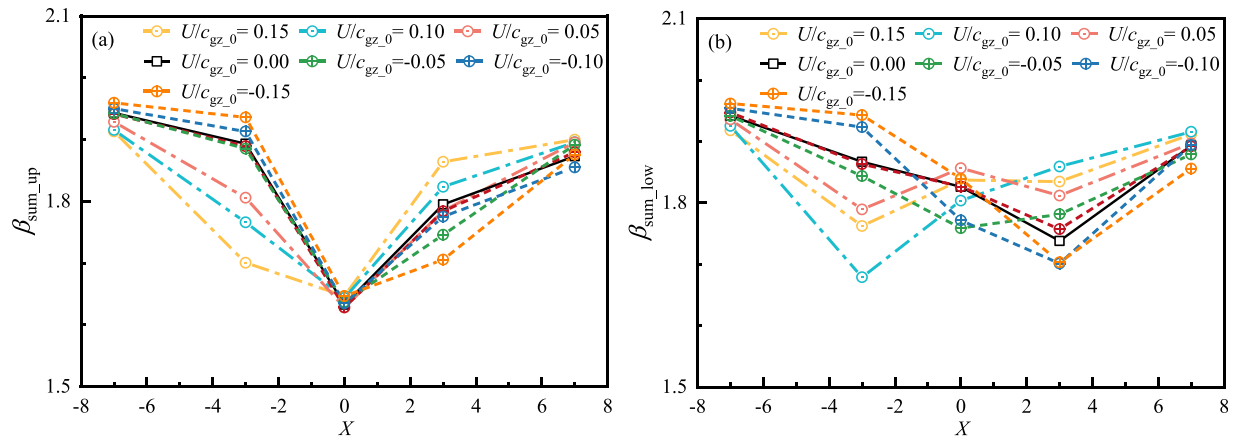
FIG. 8. Evolution of the total horizontal asymmetry of the preceding and the following influenced by water currents with various velocities. (a) Upper envelope and (b) lower envelope.

impossible to measure the energy transfer before and after the wave focus. The difference between σ_f and σ_p [obtained from Eq. (15)] influenced by various currents is consequently compared in Fig. 10. For the upper envelope in Fig. 10(a), $\Delta\sigma$ starts as a negative value, suggesting that the envelope profile presents an appearance of backward-leaning. With the waves approaching, $\Delta\sigma$ still stays negative, but different changes occurred. For instance, $\Delta\sigma$ remains stable in non-current, while increasing in the presence of the co-propagating current and decreasing in the counter-propagating current. Till the focused position, $\Delta\sigma$ increases up to slightly less than 0 in non-current as well as the counter-propagating current, while the co-propagating current forces $\Delta\sigma$ increase to the positive, implying the co-propagating current accelerates the maximum magnitude of the envelope turning to forward-leaning. After passing by, $\Delta\sigma$ becomes positive in all wave–current configurations with no deterministic pattern. This shape correction is attributed to not only the bound waves induced by wave–wave interactions local in non-current[56] but also the nonlinear superposition of the complex wave–current interaction. For the lower envelope in Fig. 10(b), as the waves propagate, most $\Delta\sigma$ decrease from negative values and

then increase to their positive maximum and finally slightly decrease. Except for the configuration with $U/c_{gz\_0} = -0.15$, the evolution process presents an approximate V-shape, with a minimum value of -0.4 appearing around the focused position. It can be pointed out that whether the process of the energy transfer between the preceding and following wave enveloped is accelerated or decelerated is determined by the current is co- or counter-propagating in the double-wave-group focusing.

IV. EVOLUTION OF SPECTRAL ENERGY DISTRIBUTION INFLUENCED BY VARIOUS CURRENTS

The Fast Fourier Transform (FFT) is adopted to investigate how undergoing currents affect the energy transfer in the process of wave focus and defocus.

A. Frequency spectrum

Figure 11 compares the spatial evolution of the spectral energy distribution influenced by various currents, where the vertical axis is normalized by the maximum amplitude in the non-current state
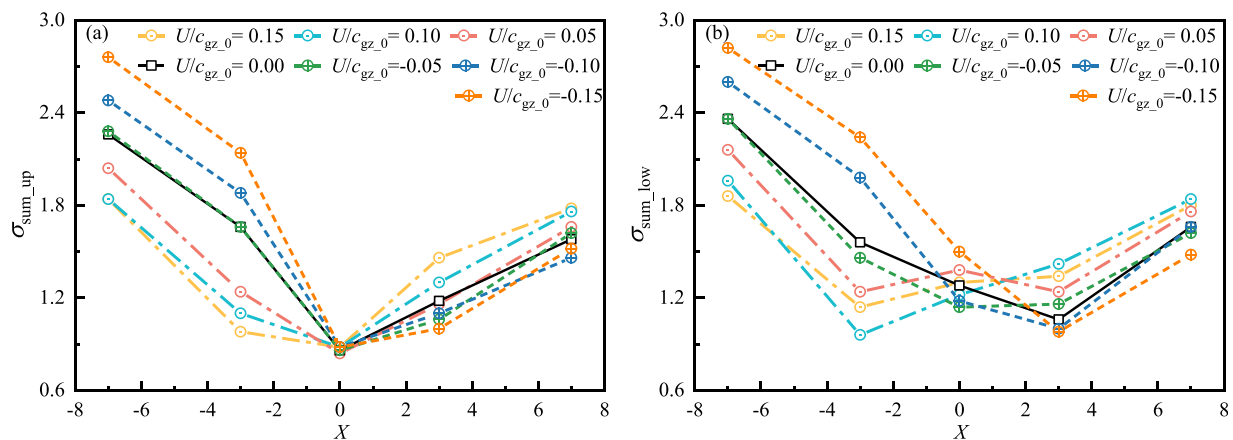

FIG. 9. Evolution of the total envelope width of the preceding and the following influenced by water currents with various velocities. (a) Upper envelope and (b) lower envelope.
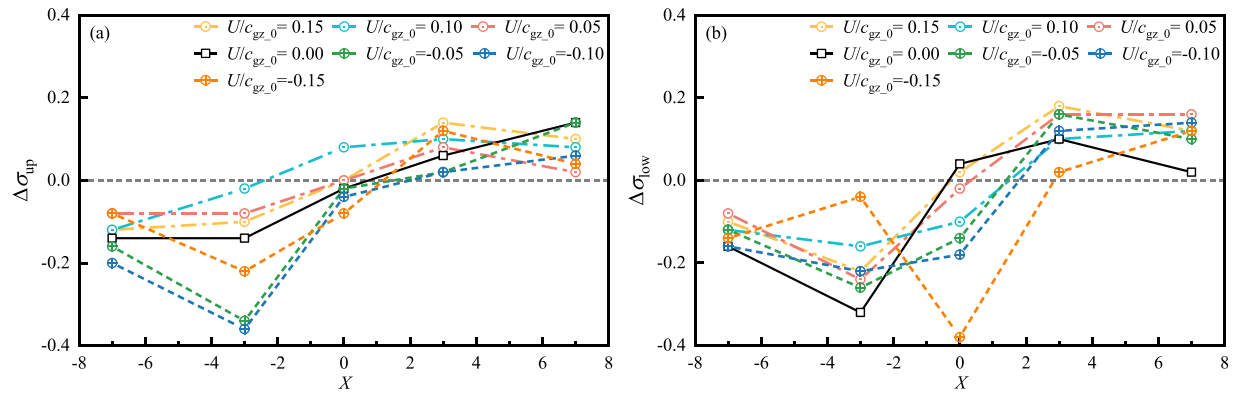
FIG. 10. Evolution of the envelope width difference between the preceding and the following influenced by water currents with various velocities. (a) Upper envelope and (b) lower envelope.

(defined as a_{max0}). The result in the absence of an underlying current is shown in Fig. 11(b) for comparison. As described in Ref. 57, the nonlinearity enlarges first and then declines with the wave evolution. The great deviation is observed in the higher frequency range (i.e., $f > 2.0\,\text{Hz}$) at the focused position, accompanied by a continuous decline in the valley between these two peaks as well as in the second peak, which is recognized as one of the typical features in the formation of extreme events.[30,58]

The underlying current plays an undeniable role in the energy transfer in double-wave-group focusing, which can be found in the enlarger partial in red shadow. It is mainly manifested as the valley between these two peaks and the second peak as well as their corresponding characteristics frequency (i.e., f_v and f_{nd} defined in Sec. II C 4). Compared to the variation in the co-propagating current [Fig. 11(a)], the magnitude of the changes in the second peak in the process of wave evolution seems more significant in the strongly counter-propagating current [such as $U/c_{gz\_0} = -0.10$ in Fig. 11(c)

and $U/c_{gz\_0} = -0.15$ in Fig. 11(d)], along with f_{nd} shifting downstream appearing as a tri-modal spectrum when two wave groups are gradually separated. This suggests that the energy returns to the initial spectral range are obstructed by the strongly counter-propagating current. In addition, an abrupt increase near $2.0\,\text{Hz}$ inclines to move to the lower frequency range as the counter-propagating current enhances, resulting from the effect of the Doppler downshift.[29]

B. Analysis of characteristic parameters

The spatial evolution of the root mean square frequency f_{rms} [obtained from Eq. (16)] is illustrated in Fig. 12. A larger f_{rms} represents a more intense nonlinear interaction. Away from the wave focus, the value of f_{rms} in the co-propagating current is a little larger for the increase in nonlinearity, resulting in the rising steepness of the wave envelope in Fig. 6(a.2). As the maximum crest appears at the focused position, the effect of current on the magnitude of the focused
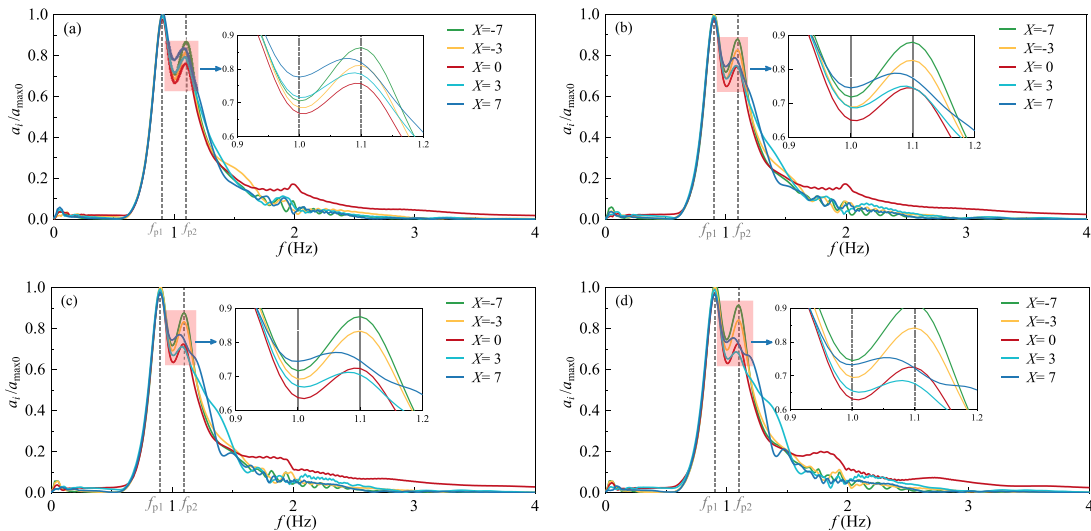

FIG. 11. Spatial evolution of the amplitude spectra in water currents with various velocities. (a) $U/c_{gz\_0} = 0.10$, (b) $U/c_{gz\_0} = 0.00$, (c) $U/c_{gz\_0} = -0.10$, and (d) $U/c_{gz\_0} = -0.15$.
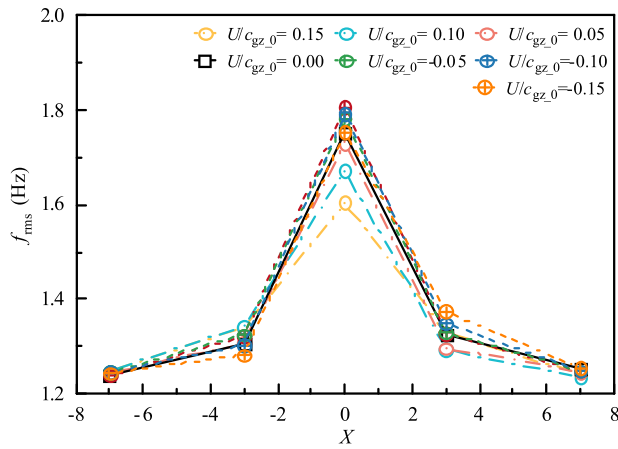
FIG. 12. Spatial evolution of the root mean square frequency influenced by water currents with various velocities.

amplitude is predicted by f_{rms}. After that, f_{rms} tends to go back to the initialization with the dotted line above other lines. The dissipation of nonlinear energy is due to the inhibition by the counter-propagating current, leading to the appearance of a steeper and narrower wave

group in Sec. III C. Finally, f_{rms} almost reduces to the initial value synchronous with the mixed field coming back to a stable state.

Statistical analysis is conducted on the evolutionary variation in the energy distribution on the valley and the second peak as well as their corresponding characteristics frequency (Fig. 13).

In Figs. 13(a.1) and 13(b.1), at seven times the characteristic wavelength before the focused position, a_v/a_{max0} and a_{nd}/a_{max0} in the co-propagating current are smaller than those in the counter-propagating current, implying that the energy transfer to higher-frequency forced by the co-propagating current has already happened at the initial stage. With the wave propagating, a_v/a_{max0} in different currents slightly reduces, and their differences decline, while a_{nd}/a_{max0} declines with faster speed than that of a_v/a_{max0}. It can be proven that more energies transfer to higher-frequency partition, promoting the frequency band upshift. Till the focused position, a_v/a_{max0} and a_{nd}/a_{max0} reach their minimum, indicating the energy transfer to the higher frequency achieves maximum. The larger the counter-propagating current velocity, the smaller the minimum, and the more energy transfer. Passing by, a_v/a_{max0} keeps increasing and tries to go back to the fundamental frequency range. While a_{nd}/a_{max0} in the strong counter-propagating current remains decreased within three times wavelength off the focused position, suggesting that the nonlinearity reduced by the counter-propagating current continues to
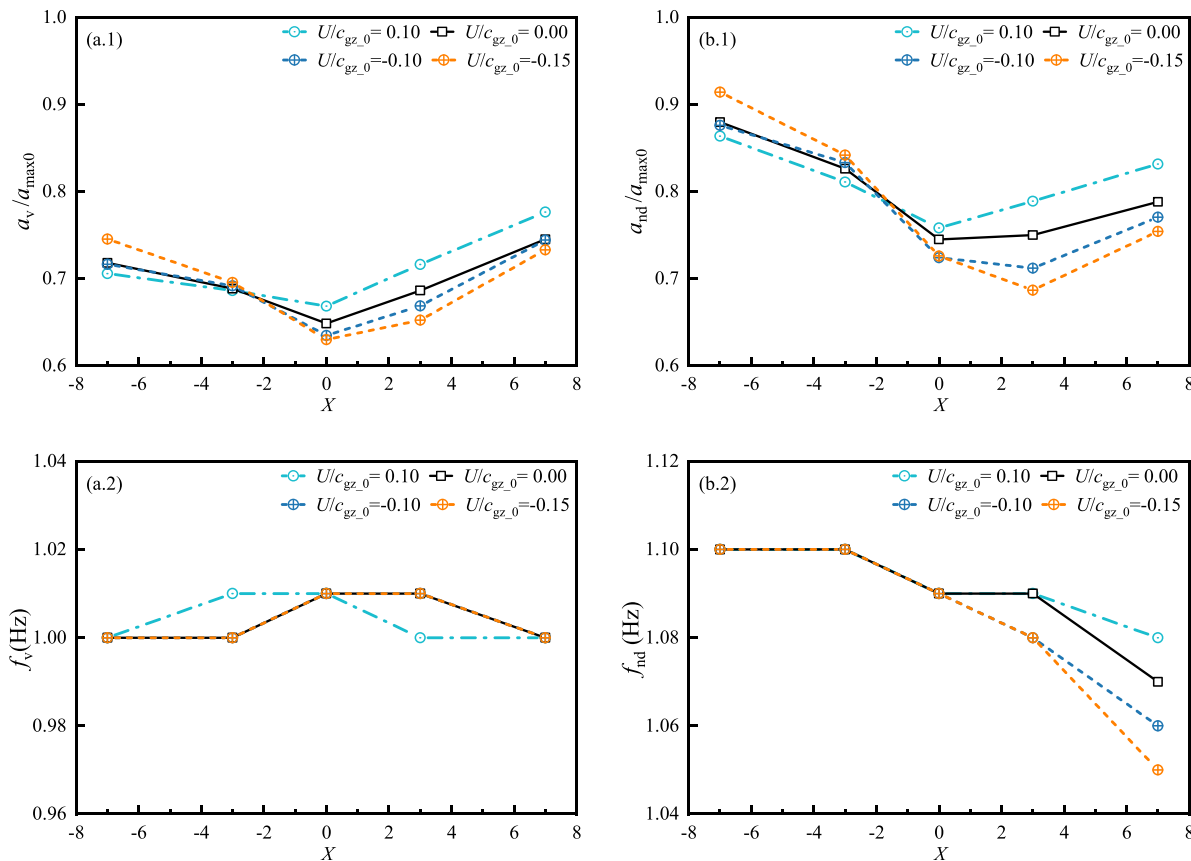

FIG. 13. Spatial evolution of energy distributions (1) and their corresponding characteristic frequencies (2) influenced by water currents with various velocities, (a) corresponding to the valley between the two peaks and (b) corresponding to the second peak.

strengthen, which is the reason that the maximum magnitude in the counter-propagating current exceeds that in non-current at that point in Fig. 7(a.1). Moreover, in the process of the energy return, the counter-propagating current with a larger velocity can induce a faster decrease (within the relative distance from 0 to 3) or a faster increase (within the relative distance from 3 to 7) of a_{nd}/a_{max0} [Fig. 13(b.1)], which is synchronous with the variation of the energy concentration in Fig. 8(a) and horizontal asymmetry in Fig. 9(a). Finally, a_v/a_{max0} and a_{nd}/a_{max0} in the counter-propagating current are still below that in the counter-propagating current. This indicates that compared to the variation in the co-propagating current, there are still more higher-frequency components remaining influenced by the counter-propagating current.

Concerning the variation of the characteristic frequency, f_v is slightly affected by different currents [Fig. 13(a.2)]. There is only a little deviation from 1.0 Hz around the focused position. For the co-propagating current, the frequency band shifts to a relatively high frequency before the focused position, while for the counter-propagating current, it occurs behind the focused position. This phenomenon may be associated with the change in the occurrence time of the crest focus and the trough focus influenced by various currents, which needs further investigation. In Fig. 13(b.2), the characteristic frequency corresponding to the second peak f_{nd} keeps consistent in all current configurations at the beginning. As the wave groups interact with each other approaching the focused position, f_{nd} decreases simultaneously at the same speed in the currents with different velocities. When the waves begin to defocus, f_{nd} in non-current and the co-propagating current keep unchanged in the first three times characteristic wavelengths, while f_{nd} in the counter-propagating current remains shifted downward at the same speed. After that, f_{nd} continues to decrease separately, with a minimum value of 1.08 Hz in the co-propagating current and 1.05 Hz in the strongly counter-propagating current. The stronger the counter-propagating current, the faster the speed of the spectral frequency band downshift.

Generally, in the process of wave defocus, the wave groups gradually separate due to different propagation velocities and the higher-frequency components decrease for the weakened interaction. From the above, under the effect of the strongly counter-propagating current, a downshift of the spectral frequency band and a decreased energy distribution (i.e., a decreased amplitude spectrum) at the second peak frequency can be observed in this process. Considering that the corresponding characteristics frequency f_{rms} also remains a little larger value for a while, this confirms that the energy transfer to the fundamental range is disturbed by the counter-propagating current with the back-flow blocked, which consequently causes a sluggish evolution. Furthermore, even if f_{rms} almost returns to the initialization, the energy distribution has undergone significant changes under the effect of the various currents besides the wave–wave interactions. For instance, a tri-model spectrum behavior appears in a strongly counter-propagating current. This also reflects that the impact of the currents on the nonlinear waves is rather than a linear superposition but more complex physics, involving irreversible changes in the dispersion relation.

V. CONCLUSIONS

In this study, the spatial evolution of the double-wave-group focusing influenced by the co- and counter-propagating current is

studied using a fully nonlinear numerical model based on the high-order spectral (HOS) method. The main conclusions are as follows:

(1) The counter-propagating current has a different impact on the focused parameters in the double-wave-group focusing from the co-propagating current, such as actual focused position, focused time, and maximum magnitude. The evolutionary process of the wave focus is significantly shortened, with a sharper crest focus followed by the trough focus, which is opposite to the co-propagating current.

(2) The horizontal asymmetry of the wave envelope varies in the spatial domain depending on the current velocity. The sum of the envelope heights β_{sum} and the sum of the envelope widths σ_{sum} decrease first and then increase as the waves focus and defocus, with the minimum at the focused position. In the counter-propagating current, the decreased speeds of β_{sum} and σ_{sum} can be accelerated before wave focuses with the increased speeds decelerated after wave focus and the transition from the backward-leaning (negative $\Delta\sigma$) to the forward-leaning (positive $\Delta\sigma$) is also delayed.

(3) The influence of the underlying current on the energy transfer in the evolution of the double-wave-group focusing is analyzed. It manifested as the irreversible variation of the valley between these two peaks and the second peak as well as their corresponding characteristics frequency (f_v and f_{nd}), which aids in clarifying the spatial evolution of the wave envelope profile influenced by various currents.

(4) In the process of wave defocus, energy transfer to the fundamental range is disturbed by the counter-propagating current with the back-flow blocked, consequently causing a sluggish evolution. It can be deduced from the phenomenon that a downshift of the spectral frequency band, and a decreased energy distribution at the second peak frequency, as well as the corresponding characteristics frequency f_{rms} also remain a little larger value for a while in the strongly counter-propagating current.

(5) The impact of the currents on the nonlinear waves is rather than a linear superposition but more complex physics. Even if the root mean square frequency f_{rms} almost returns to the initialization, the energy distribution has undergone significant changes under the effect of the various currents besides the wave–wave interactions, like a tri-model spectrum behavior appearing after wave focus in a strongly counter-propagating current.

The above findings explain the spatial evolution of the double-wave-group focusing influenced by the co- and counter-propagating currents. It helps to understand the mechanisms of wave–current interactions and even extreme wave formation. In future work, more unknown but fascinating physical processes could be promoted, such as non-uniform (in space) current interacting with focused waves, sheer current interacting with extreme waves, and so on.

ACKNOWLEDGMENTS

28 November 2025 04:30:49

AUTHOR DECLARATIONS
Conflict of Interest

The authors have no conflicts to disclose.

Author Contributions

Kanglixi Ding: Conceptualization (equal); Data curation (equal); Investigation (equal); Methodology (equal); Visualization (equal); Writing – original draft (equal). **Binzhen Zhou:** Funding acquisition (equal); Project administration (equal); Supervision (lead); Writing – review & editing (equal). **Yi Xiao:** Formal analysis (equal); Investigation (equal); Writing – review & editing (equal). **Lei Wang:** Conceptualization (lead); Formal analysis (equal); Funding acquisition (equal); Methodology (lead); Writing – review & editing (lead). **Huabin Shi:** Investigation (equal); Writing – review & editing (equal).

DATA AVAILABILITY

The data that support the findings of this study are available from the corresponding author upon reasonable request.

REFERENCES

[1]K. Zhu, H. Shi, J. Tao et al., "Analytical study on hydrodynamic performance of co-located offshore wind–solar farms," Phys. Fluids **36**(1), 013325 (2024).

[2]C. Zhang, P. Wang, L. Huang et al., "Resonance mechanism of hydroelastic response of multi-patch floating photovoltaic structure in water waves over stepped seabed," Phys. Fluids **35**(10), 107137 (2023).

[3]E. Didenkulova, I. Didenkulova, and I. Medvedev, "Freak wave events in 2005–2021: Statistics and analysis of favourable wave and wind conditions," Nat. Hazards Earth Syst. Sci. Discuss. **2022**, 1–17.

[4]L. Chen, D. Stagonas, H. Santo et al., "Numerical modelling of interactions of waves and sheared currents with a surface piercing vertical cylinder," Coastal Eng. **145**, 65–83 (2019).

[5]Y. Li and A. Chabchoub, "How currents trigger extreme sea waves. The roles of Stokes drift, Eulerian return flow, and a background flow in the open ocean," Geophys. Res. Lett. **51**(6), e2023GL107381, https://doi.org/10.1029/2023GL107381 (2024).

[6]B. Liao, G. Dong, Y. Ma et al., "Modified nonlinear Schrödinger equation for gravity waves with the influence of wind, currents, and dissipation," Phys. Fluids **35**(3), 037103 (2023).

[7]H. Halsne, A. Benetazzo, F. Barbariol et al., "Wave modulation in a strong tidal current and its impact on extreme waves," J. Phys. Oceanogr. **54**(1), 131–151 (2024).

[8]B. Zhou, K. Ding, J. Huang et al., "Influence of uniform currents on nonlinear characteristics of double-wave-group focusing," Phys. Fluids **36**(3), 037125 (2024).

[9]L. Wang, K. Ding, B. Zhou et al., "Quantitative prediction of the freak wave occurrence probability in co-propagating mixed waves," Ocean Eng. **271**, 113810 (2023).

[10]L. Wang, J. Li, S. Liu et al., "Statistics of long-crested extreme waves in single and mixed sea states," Ocean Dyn. **71**, 21–42 (2021).

[11]G. Lindgren, "Some properties of a normal process near a local maximum," Ann. Math. Stat. **41**(6), 1870–1883 (1970).

[12]T. B. Johannessen and C. Swan, "A laboratory study of the focusing of transient and directionally spread surface water waves," Proc. R. Soc. London A **457**(2008), 971–1006 (2001).

[13]T. E. Baldock, C. Swan, and P. H. Taylor, "A laboratory study of nonlinear surface waves on water," Philos. Trans. R. Soc. London. Ser. A: Math. Phys. Eng. Sci. **354**(1707), 649–676 (1996).

[14]J. L. Hammack, D. M. Henderson, and H. Segur, "Progressive waves with persistent two-dimensional surface patterns in deep water," J. Fluid Mech. **532**, 1–52 (2005).

[15]X. Li, X. Li, and S. Liao, "Pattern transition of two-dimensional Faraday waves at an extremely shallow depth," Sci. China Math. **59**(11), 1–3 (2016).

[16]X. Li, J. Li, X. Li, S. Liao, and C. Chen, "Effect of width on the properties of Faraday waves in Hele-Shaw cells," Sci. China Phys. Mech. Astron. **62**(7), 1–6 (2019).

[17]R. H. Gibbs and P. H. Taylor, "Formation of walls of water in 'fully' nonlinear simulations," Appl. Ocean Res. **27**(3), 142–157 (2005).

[18]T. Adcock, R. Gibbs, and P. Taylor, "The nonlinear evolution and approximate scaling of directionally spread wave groups on deep water," Proc. R. Soc. A **468**(2145), 2704–2721 (2012).

[19]A. Babanin, D. Chalikov, I. Young et al., "Predicting the breaking onset of surface water waves," Geophys. Res. Lett. **34**(7), L07605, https://doi.org/10.1029/2006GL029135 (2007).

[20]M. Perlin, W. Choi, and Z. Tian, "Breaking waves in deep and intermediate waters," Annu. Rev. Fluid Mech. **45**, 115–145 (2013).

[21]T. Adcock, P. Taylor, and S. Draper, "Nonlinear dynamics of wave-groups in random seas: Unexpected walls of water in the open ocean," Proc. R. Soc. A **471**(2184), 20150660 (2015).

[22]T. A. A. Adcock, P. H. Taylor, and S. Draper, "On the shape of large wave-groups on deep water—The influence of bandwidth and spreading," Phys. Fluids **28**(10), 106601 (2016).

[23]T. Tang, P. Tromans, and T. Adcock, "Field measurement of nonlinear changes to large gravity wave groups," J. Fluid Mech. **873**, 1158–1178 (2019).

[24]T. Tang and T. Adcock, "The influence of finite depth on the evolution of extreme wave statistics in numerical wave tanks," Coastal Eng. **166**, 103870 (2021).

[25]T. Tang, W. Xu, D. Barratt et al., "Spatial evolution of the kurtosis of steep unidirectional random waves," J. Fluid Mech. **908**, A3 (2021).

[26]I. Lavrenov and A. Porubov, "Three reasons for freak wave generation in the non-uniform current," Eur. J. Mech.-B/Fluids **25**(5), 574–585 (2006).

[27]I. Brevik and A. Bjørn, "Flume experiment on waves and currents. I. Rippled bed," Coastal Eng. **3**, 149–177 (1979).

[28]M. Onorato, D. Proment, and A. Toffoli, "Triggering rogue waves in opposing currents," Phys. Rev. Lett. **107**(18), 184502 (2011).

[29]G. Ducrozet, M. Abdolahpour, F. Nelli et al., "Predicting the occurrence of rogue waves in the presence of opposing currents with a high-order spectral method," Phys. Rev. Fluids **6**(6), 064803 (2021).

[30]B. Liao, Y. Ma, X. Ma et al., "Experimental study on the evolution of Peregrine breather with uniform-depth adverse currents," Phys. Rev. E **97**(5), 053102 (2018).

[31]J. Li, D. Liu, and S. Liu, "Numerical investigation of the effect of current on wave focusing," China Ocean Eng. **26**, 37–48 (2012).

[32]D. Merkoune, J. Touboul, N. Abcha et al., "Focusing wave group on a current of finite depth," Nat. Hazards Earth Syst. Sci. **13**(11), 2941–2949 (2013).

[33]J. Wang, Q. Ma, and S. Yan, "A fully nonlinear numerical method for modeling wave–current interactions," J. Comput. Phys. **369**, 173–190 (2018).

[34]H. Fang, P. Liu, L. Tang et al., "The theory of fifth-order Stokes waves in a linear shear current," Proc. R. Soc. A **479**(2280), 20230565 (2023).

[35]S. Å. Ellingsen, Z. Zheng, M. Abid et al., "Dispersive wave focusing on a shear current: Part 1—Linear approximations," Water Waves (published online).

[36]C. Soares, "On the occurrence of double peaked wave spectra," Ocean Eng. **18**(1–2), 167–171 (1991).

[37]R. Vettor and C. Soares, "A global view on bimodal wave spectra and crossing seas from ERA-interim," Ocean Eng. **210**, 107439 (2020).

[38]F. Arena and C. Soares, "Nonlinear high wave groups in bimodal sea states," J. Waterway Port Coastal Ocean Eng. **135**(3), 69–79 (2009).

[39]L. Wang, K. Ding, B. Zhou et al., "Nonlinear statistical characteristics of the multi-directional waves with equivalent energy," Phys. Fluids **35**(8), 087101 (2023).

[40]B. Zhou, K. Ding, J. Wang *et al.*, "Experimental study on the interactions between wave groups in double-wave-group focusing," Phys. Fluids **35**(3), 037118 (2023).

[41]Z. Xin, X. Li, and Y. Li, "Coupled effects of wave and depth-dependent current interaction on loads on a bottom-fixed vertical slender cylinder," Coastal Eng. **183**, 104304 (2023).

[42]G. Ducrozet, F. Bonnefoy, D. Le Touzé *et al.*, "A modified high-order spectral method for wavemaker modeling in a numerical wave tank," Eur. J. Mech.-B/Fluids **34**, 19–34 (2012).

[43]Y. Pan, "On the model formulations for the interaction of nonlinear waves and current," Wave Motion **96**, 102587 (2020).

[44]Y. Agnon and H. Bingham, "A non-periodic spectral method with application to nonlinear water waves," Eur. J. Mech.-B/Fluids **18**(3), 527–534 (1999).

[45]D. Dommermuth and D. Yue, "A high-order spectral method for the study of nonlinear gravity waves," J. Fluid Mech. **184**, 267–288 (1987).

[46]B. West, K. Brueckner, R. Janda *et al.*, "A new numerical method for surface hydrodynamics," J. Geophys. Res. **92**(C11), 11803–11824, https://doi.org/10.1029/JC092iC11p11803 (1987).

[47]F. Bonnefoy, D. Le Touzé, and P. Ferrant, "A fully-spectral 3D time-domain model for second-order simulation of wavetank experiments. Part B: Validation, calibration versus experiments and sample applications," Appl. Ocean Res. **28**(2), 121–132 (2006).

[48]Z. Liu, Z. Lin, L. Tao *et al.*, "Nonlinear wave–current interaction in water of finite depth," J. Waterway Port Coastal Ocean Eng. **142**(6), 04016009 (2016).

[49]G. Rodriguez, C. Soares, M. Pacheco *et al.*, "Wave height distribution in mixed sea states," J. Offshore Mech. Arct. Eng. **124**(1), 34–40 (2002).

[50]E. Buldakov, D. Stagonas, and R. Simons, "Extreme wave groups in a wave flume: Controlled generation and breaking onset," Coastal Eng. **128**, 75–83 (2017).

[51]Y. Goda, "A comparative review on the functional forms of directional wave spectrum," Coastal Eng. J. **41**(1), 1–20 (1999).

[52]R. Fu, G. Wang, J. Zheng *et al.*, "Statistical properties of group energy and group duration for unidirectional ocean wave groups," Ocean Eng. **266**, 112786 (2022).

[53]R. Fu, Y. Ma, G. Dong *et al.*, "A wavelet-based wave group detector and predictor of extreme events over unidirectional sloping bathymetry," Ocean Eng. **229**, 108936 (2021).

[54]M. Tayfun and J. Lo, "Nonlinear effects on wave envelope and phase," J. Waterway Port Coastal Ocean Eng. **116**(1), 79–100 (1990).

[55]L. Mandel, "Interpretation of instantaneous frequencies," Am. J. Phys. **42**(10), 840–846 (1974).

[56]C. Cui and W. Pan, "Experimental study on the wavelengths of two-dimensional and three-dimensional freak waves," China Ocean Eng. **37**(1), 154–164 (2023).

[57]L. Wang, J. Li, S. Liu *et al.*, "Experimental and numerical studies on the focused waves generated by double wave groups," Front. Energy Res. **8**, 133 (2020).

[58]J. Liu, X. Feng, and J. Cui, "Experimental study of extreme waves based on nonlinear Schrödinger equation under background of a random sea," Phys. Fluids **35**(4), 047118 (2023).